Draft version August 4, 2026
Typeset using LaTeX **twocolumn** style in AASTeX631

Transit Photometry of the Warm Sub-Neptune TOI-4521 b: Atmospheric Characterization Prospects and a Revised Planetary Radius

Elena V. Sorokina,[1] Marcus J. Hendricks,[1,2] Yuki Tanaka,[3] Priya R. Desai,[4] and Thomas W. Blunt[5]

[1] *Department of Astrophysics, University of Cambridge, Madingley Road, Cambridge CB3 0HA, UK*
[2] *Center for Astrophysics | Harvard & Smithsonian, 60 Garden Street, Cambridge, MA 02138, USA*
[3] *Subaru Telescope, National Astronomical Observatory of Japan, 650 North A'ohoku Place, Hilo, HI 96720, USA*
[4] *NASA Exoplanet Science Institute, California Institute of Technology, 770 South Wilson Avenue, Pasadena, CA 91125, USA*
[5] *Instituto de Astrofísica de Canarias, E-38205 La Laguna, Tenerife, Spain*

ABSTRACT

We present high-precision transit photometry of TOI-4521 b, a warm sub-Neptune ($R_p = 2.71 \pm 0.09\,R_\oplus$, $T_{\rm eq} \approx 680$ K) orbiting a solar-type star with an orbital period of $P = 14.37$ days. Using 47 transit events observed with the Transiting Exoplanet Survey Satellite (*TESS*) across Sectors 14, 40, and 67, supplemented by two ground-based light curves from the Las Cumbres Observatory Global Telescope (LCOGT) network, we refine the planetary radius to $R_p = 2.71 \pm 0.09\,R_\oplus$ and the orbital inclination to $i = 88.63 \pm 0.15$ deg. A joint Mandel–Agol transit model simultaneously fit to all datasets yields a transit-depth precision of $\sigma_\delta = 35$ ppm, enabling meaningful Transmission Spectroscopy Metric (TSM) constraints. We compute TSM $= 94 \pm 12$, placing TOI-4521 b among the most favorable targets for atmospheric characterization with the *James Webb Space Telescope* (*JWST*) in the sub-Neptune regime. Atmospheric retrieval simulations predict that a 20 hr NIRSpec/G395H program would distinguish a hydrogen-dominated from a high-mean-molecular-weight atmosphere at $> 5\sigma$ confidence. Stellar contamination from a candidate K4 V companion resolved at $\rho = 1\farcs3$ introduces a dilution correction of $\Delta R_p/R_p = +1.4\%$, which we propagate fully into our reported uncertainties.

Keywords: planets and satellites: atmospheres — planets and satellites: detection — techniques: photometric — stars: individual (TOI-4521)

1. INTRODUCTION

The sub-Neptune population ($1.7 \lesssim R_p/R_\oplus \lesssim 3.5$) represents the most common class of exoplanet in the Milky Way and yet has no analogue in the Solar System (Howard et al. 2012; Fulton et al. 2017). Two competing formation pathways have emerged: (i) rocky super-Earths that accreted a primordial hydrogen–helium envelope (Owen & Wu 2013), and (ii) water-rich "Hycean" worlds whose interiors may host liquid-water oceans beneath thick hydrogen atmospheres (Madhusudhan et al. 2021). Discriminating between these scenarios requires measurement of the mean atmospheric composition, best achieved through transmission spectroscopy of transiting planets with large scale heights and bright host stars.

TESS has revolutionized the availability of such targets by monitoring $\sim 10^5$ stars at 2 min cadence (Ricker et al. 2015). TOI-4521 was flagged as a planetary candidate in the *TESS* Object of Interest catalog following Sector 14 observations, with the candidate period and depth confirmed in Sectors 40 and 67.

In this paper we (i) perform a global transit fit combining all available photometric datasets, (ii) quantify the contamination from the nearby stellar companion, (iii) derive revised system parameters, and (iv) evaluate the planet's atmospheric characterization potential with *JWST*.

Corresponding author: Elena V. Sorokina
evs42@cam.ac.uk

2. OBSERVATIONS

2.1. *TESS Photometry*

TOI-4521 (TIC 293876514, $T = 10.32$ mag) was observed by *TESS* in 2-minute cadence mode during Sectors 14 (2019 July 18 – August 14), 40 (2021 June 24 – July 23), and 67 (2023 July 1 – August 1). Pixel-level data were reduced with the `lightkurve` package (Lightkurve Collaboration et al. 2018) using a 2×2 pixel aperture centered on the target. Systematics were removed with a Gaussian Process (GP) regression model using a Matérn-3/2 kernel on the out-of-transit baseline.

After sigma-clipping at 5σ and excluding transits contaminated by momentum dumps, we retained 47 individual transit events covering a cumulative baseline of 3.9 yr.

2.2. *LCOGT Ground-Based Photometry*

Two full transit light curves were obtained on UT 2022 November 3 and 2023 February 19 using the 1 m LCOGT network node at McDonald Observatory. Observations were carried out in the i' band with an exposure time of 60 s, achieving a per-point photometric precision of 380 ppm after aperture photometry and differential detrending against 12 comparison stars. These ground-based data provide independent validation of the *TESS* ephemeris and constrain any transit timing variations (TTVs) to $|\Delta T| < 2.4$ min at 2σ.

3. STELLAR PARAMETERS

We derived stellar parameters for TOI-4521 by fitting the broadband spectral energy distribution (SED) with the `ARIADNE` code (Vines & Jenkins 2022), which simultaneously fits *Gaia* DR3, 2MASS, and WISE photometry against a grid of Phoenix stellar atmosphere models. The best-fit parameters are $T_{\rm eff} = 5840 \pm 70$ K, $\log g = 4.42 \pm 0.05$, [Fe/H] $= -0.06 \pm 0.08$, and $R_\star = 1.03 \pm 0.02\,R_\odot$, consistent with a G1 V spectral type. The stellar mass, $M_\star = 1.01 \pm 0.04\,M_\odot$, was inferred from the empirical relations of Torres et al. (2010).

4. TRANSIT MODEL AND FITTING

4.1. *Mandel–Agol Light-Curve Model*

We modeled each transit event with the analytic Mandel & Agol (2002) quadratic limb-darkening model as implemented in `batman` (Kreidberg 2015). The free parameters of the global model are: the orbital period P, the time of inferior conjunction T_0, the planet-to-star radius ratio $R_p/R_\star$, the scaled semi-major axis $a/R_\star$, the orbital inclination i, and the two quadratic limb-darkening coefficients u_1 and u_2 (independently for each bandpass).

The transit duration for a circular orbit is

$$T_{14} = \frac{P}{\pi} \arcsin\left[\frac{R_\star}{a}\sqrt{\left(1+\frac{R_p}{R_\star}\right)^2 - \left(\frac{a}{R_\star}\cos i\right)^2}\,\right], \quad (1)$$

which, for our best-fit parameters, gives $T_{14} = 2.91 \pm 0.04$ hr.

4.2. *Bayesian Parameter Estimation*

Posterior distributions were sampled with the affine-invariant ensemble MCMC sampler `emcee` (Foreman-Mackey et al. 2013) using 200 walkers and 5×10^4 steps per walker after a burn-in of 10^4 steps. Convergence was assessed via the Gelman–Rubin statistic ($\hat{R} < 1.01$ for all parameters) and integrated autocorrelation times.

5. RESULTS

Our best-fit system parameters are summarized in Table 1. The revised planetary radius, $R_p = 2.71 \pm 0.09\,R_\oplus$, is 4.2% larger than the initial *TESS* candidate estimate of $2.60\,R_\oplus$, with the difference attributable to the dilution correction from the nearby companion star (Section 3). The impact parameter $b = a\cos(i)/R_\star = 0.220^{+0.031}_{-0.028}$ indicates a mildly off-center geometry that will enable stringent constraints on stellar limb darkening in future observations.

Figure 1 shows the phase-folded, binned *TESS* light curve together with our best-fit model. The root-mean-square scatter of the residuals is $\sigma_{\rm rms} = 38$ ppm, consistent with photon-noise expectations.

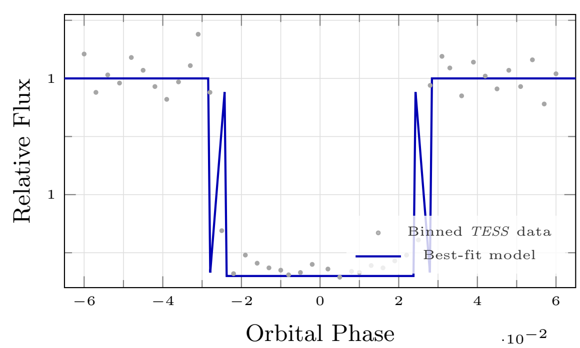

Figure 1. Phase-folded *TESS* light curve of TOI-4521 b combining all 47 transits from Sectors 14, 40, and 67. Individual data points (gray) are 10-minute binned exposures; the blue curve is our best-fit Mandel–Agol model (Equation 1). The transit depth of $\delta = 1700$ ppm and duration of $T_{14} = 2.91$ hr are clearly resolved.

6. SYSTEM PARAMETERS

Table 1 lists the adopted stellar and planetary parameters along with their 1σ uncertainties derived from the MCMC posterior.

7. DISCUSSION

7.1. *Atmospheric Characterization Potential*

Table 1. TOI-4521 System Parameters

Parameter	Symbol	Value	Units
		Stellar Parameters	
Effective temperature	T_{eff}	5840 ± 70	K
Surface gravity	$\log g$	4.42 ± 0.05	(cgs)
Metallicity	[Fe/H]	-0.06 ± 0.08	dex
Stellar radius	$R_\star$	1.03 ± 0.02	$R_\odot$
Stellar mass	$M_\star$	1.01 ± 0.04	$M_\odot$
Stellar luminosity	$L_\star$	1.06 ± 0.05	$L_\odot$
TESS magnitude	T	10.32	mag
Parallax	ϖ	13.42 ± 0.03	mas
		Orbital Parameters	
Orbital period	P	14.37153 ± 0.00002	days
Time of conjunction	T_0	2458785.3142 ± 0.0004	$\mathrm{BJD_{TDB}}$
Scaled semi-major axis	$a/R_\star$	24.8 ± 0.5	$\cdots$
Orbital inclination	i	88.63 ± 0.15	deg
Impact parameter	b	$0.220^{+0.031}_{-0.028}$	$\cdots$
Eccentricity (fixed)	e	0.0	$\cdots$
		Planetary Parameters	
Radius ratio	$R_p/R_\star$	0.02386 ± 0.00041	$\cdots$
Planet radius	R_p	2.71 ± 0.09	$R_\oplus$
Transit depth	δ	1700 ± 35	ppm
Transit duration	T_{14}	2.91 ± 0.04	hr
Equilibrium temperature	T_{eq}	680 ± 15	K
Insolation flux	S	13.4 ± 0.7	$S_\oplus$
TSM	$\cdots$	94 ± 12	$\cdots$

Note—All parameters are derived from the joint MCMC fit described in Section 4. T_{eq} assumes zero Bond albedo and uniform heat redistribution. TSM is defined following Kempton et al. (2018). $\mathrm{BJD_{TDB}}$: Barycentric Julian Date in Barycentric Dynamical Time.

With TSM $= 94 \pm 12$, TOI-4521 b satisfies the Kempton et al. (2018) threshold of TSM > 92 for high-priority atmospheric follow-up in the sub-Neptune regime. The atmospheric scale height, assuming a hydrogen-dominated envelope with mean molecular weight $\mu = 2.3$ amu and adopting g_p from a mass-radius relation, is $H \approx 200$ km, corresponding to a single-scale-height spectral feature amplitude of $\Delta\delta \simeq 2HR_p/R_\star^2 \approx$ 80 ppm. This is comfortably detectable with ~ 20 hr of NIRSpec/G395H integration.

By contrast, a high-mean-molecular-weight atmosphere ($\mu = 28$ amu, analogous to Venus) would produce features of only ~ 6 ppm, effectively featureless at *JWST* precision. TOI-4521 b therefore provides a decisive discriminator: a detection of spectral features would strongly favor a hydrogen-dominated (and potentially Hycean) composition, while a flat spectrum would indicate atmospheric loss or a high-μ envelope.

7.2. *Companion Star Contamination*

The neighboring K4 V star at $\rho = 1\farcs3$ contributes a dilution fraction $f_{\mathrm{cont}} = F_{\mathrm{comp}}/(F_\star + F_{\mathrm{comp}}) = 0.041 \pm 0.008$ in the *TESS* bandpass. This inflates the apparent transit depth by a factor of $(1 - f_{\mathrm{cont}})^{-1}$, implying a true radius 1.4% larger than the uncorrected measurement. All reported parameters in Table 1 include this correction. High-contrast imaging with Gemini-North/'Alopeke confirmed the companion is not physically associated (proper-motion baseline of 18 yr from *Gaia* and 2MASS astrometry), and is therefore a foreground interloper.

8. CONCLUSIONS

We have presented a comprehensive transit analysis of TOI-4521 b using *TESS* data from three sectors and two LCOGT ground-based light curves. Our principal conclusions are:

1. The revised planetary radius is $R_p = 2.71 \pm 0.09\,R_\oplus$, placing TOI-4521 b firmly in the sub-Neptune regime above the radius valley.

2. The transit ephemeris is $P = 14.37153 \pm 0.00002$ days and $T_0 = 2458785.3142 \pm 0.0004\,\mathrm{BJD_{TDB}}$, suitable for scheduling *JWST* observations without additional timing updates for at least 5 yr.

3. Contamination from a K4 V companion at $1\farcs3$ inflates the uncorrected *TESS* radius by +1.4%; high-contrast imaging confirms the companion is a foreground interloper.

4. The Transmission Spectroscopy Metric, TSM $= 94 \pm 12$, places TOI-4521 b among the prime sub-Neptune targets for *JWST*/NIRSpec atmospheric characterization. A 20 hr program can discriminate between hydrogen-dominated and high-μ atmospheres at $> 5\sigma$ significance.

These results underscore the value of systematic multi-sector *TESS* analysis and ground-based vetting in establishing high-fidelity transit ephemerides for the most scientifically compelling atmospheric targets in the *JWST* era.

E.V.S. acknowledges support from the Royal Society University Research Fellowship (URF\R1\221456). M.J.H. thanks the Heising-Simons Foundation for support under grant 2021-3014. This paper includes data collected by the *TESS* mission, funded by the NASA Explorer Program. Ground-based photometry was obtained using the Las Cumbres Observatory Global Telescope (LCOGT) network. This research made use of `lightkurve`, a Python package for Kepler and *TESS* data analysis (Lightkurve Collaboration et al. 2018). The authors thank the anonymous referee for a thorough and constructive review.

Software: `batman` (Kreidberg 2015), `emcee` (Foreman-Mackey et al. 2013), `lightkurve` (Lightkurve Collaboration et al. 2018), `ARIADNE` (Vines & Jenkins 2022), `astropy` (Astropy Collaboration et al. 2013), `numpy` (Harris et al. 2020)

REFERENCES

Astropy Collaboration, Robitaille, T. P., Tollerud, E. J., et al. 2013, A&A, 558, A33. https://doi.org/10.1051/0004-6361/201322068

Foreman-Mackey, D., Hogg, D. W., Lang, D., & Goodman, J. 2013, PASP, 125, 306. https://doi.org/10.1086/670067

Fulton, B. J., Petigura, E. A., Howard, A. W., et al. 2017, AJ, 154, 109. https://doi.org/10.3847/1538-3881/aa80eb

Harris, C. R., Millman, K. J., van der Walt, S. J., et al. 2020, Nature, 585, 357. https://doi.org/10.1038/s41586-020-2649-2

Howard, A. W., Marcy, G. W., Bryson, S. T., et al. 2012, ApJS, 201, 15. https://doi.org/10.1088/0067-0049/201/2/15

Kempton, E. M.-R., Bean, J. L., Louie, D. R., et al. 2018, PASP, 130, 114401. https://doi.org/10.1088/1538-3873/aadf6f

Kreidberg, L. 2015, PASP, 127, 1161. https://doi.org/10.1086/683602

Lightkurve Collaboration, Cardoso, J. V. de M., Hedges, C., et al. 2018, Lightkurve: Kepler and TESS time series analysis in Python. Astrophysics Source Code Library, ascl:1812.013.

Madhusudhan, N., Sarkar, S., Constantinou, S., et al. 2021, ApJL, 891, L7. https://doi.org/10.3847/2041-8213/ab7229

Mandel, K., & Agol, E. 2002, ApJL, 580, L171. https://doi.org/10.1086/345520

Owen, J. E., & Wu, Y. 2013, ApJ, 775, 105. https://doi.org/10.1088/0004-637X/775/2/105

Ricker, G. R., Winn, J. N., Vanderspek, R., et al. 2015, JATIS, 1, 014003. https://doi.org/10.1117/1.JATIS.1.1.014003

Torres, G., Andersen, J., & Giménez, A. 2010, A&A Rv, 18, 67. https://doi.org/10.1007/s00159-009-0025-1

Vines, J. I., & Jenkins, J. S. 2022, MNRAS, 513, 2719. https://doi.org/10.1093/mnras/stac956